REPORT DOCUMENTATION PAGE

Form Approved
OMB No. 0704-0188

1. REPORT DATE *(DD-MM-YYYY)*	2. REPORT TYPE	3. DATES COVERED *(From - To)*
6-09-2007	Technical Paper	

4. TITLE AND SUBTITLE

Total and Differential Sputter Yields of Boron Nitride Measured by Quartz Crystal Microbalance and Weight Loss (Preprint)

5a. CONTRACT NUMBER

5b. GRANT NUMBER

5c. PROGRAM ELEMENT NUMBER

6. AUTHOR(S)
Binyamin Rubin, James L. Topper and Azer P. Yalin (Colorado State Univ)

5d. PROJECT NUMBER

5e. TASK NUMBER
48470052

5f. WORK UNIT NUMBER

7. PERFORMING ORGANIZATION NAME(S) AND ADDRESS(ES)

Air Force Research Laboratory (AFMC)
AFRL/PRSS
1 Ara Drive
Edwards AFB CA 93524-7013

8. PERFORMING ORGANIZATION REPORT NUMBER

AFRL-PR-ED-TP-2007-406

9. SPONSORING / MONITORING AGENCY NAME(S) AND ADDRESS(ES)

Air Force Research Laboratory (AFMC)
AFRL/PRS
5 Pollux Drive
Edwards AFB CA 93524-7048

10. SPONSOR/MONITOR'S ACRONYM(S)

11. SPONSOR/MONITOR'S NUMBER(S)
AFRL-PR-ED-TP-2007-406

12. DISTRIBUTION / AVAILABILITY STATEMENT

Approved for public release; distribution unlimited (PA #07939A).

13. SUPPLEMENTARY NOTES

For presentation at the 30th International Electric Propulsion Conference (2007 IEPC), Florence Italy, 17-20 Sep 2007. IEPC-2007-074.

14. ABSTRACT

We present results of differential sputter yield measurements of HBC and HBR grades of boron nitride due to bombardment by xenon ions. Total sputter yield measurements are made using a weight loss approach. Differential sputter yield measurements (of condensable components) are made using a quartz crystal microbalance (QCM). The QCM measurement allows full angular resolution, i.e. differential sputtering yield measurements are measured as a function of both polar angle and azimuthal angle. Measured profiles are presented for 100, 250, 350 and 500 eV Xe+ bombardment at 0º, 15º, 30º and 45º angles of incidence. We fit the measured profiles with Modified Zhang expressions using two free parameters: the total sputter yield, Y, and characteristic energy E*. Sputtering of HBC versus HBR grades of BN is compared, as is results of sputter measurements from the weight loss versus QCM approaches. Finally, effects of sample moisture absorption are considered.

15. SUBJECT TERMS

16. SECURITY CLASSIFICATION OF:			17. LIMITATION OF ABSTRACT	18. NUMBER OF PAGES	19a. NAME OF RESPONSIBLE PERSON
a. REPORT	b. ABSTRACT	c. THIS PAGE			Dr. Justin W. Koo
Unclassified	**Unclassified**	**Unclassified**	SAR	14	19b. TELEPHONE NUMBER *(include area code)* N/A

Total and Differential Sputter Yields Of Boron Nitride Measured by Quartz Crystal Microbalance and Weight Loss (PREPRINT)

IEPC-2007-074

Presented at the 30th International Electric Propulsion Conference, Florence, Italy, September 17 –September 20, 2007

Binyamin Rubin*, James L. Topper†, Azer P. Yalin‡
Colorado State University, Fort Collins, Colorado, 80523

Abstract: We present results of differential sputter yield measurements of HBC and HBR grades of boron nitride due to bombardment by xenon ions. Total sputter yield measurements are made using a weight loss approach. Differential sputter yield measurements (of condensable components) are made using a quartz crystal microbalance (QCM). The QCM measurement allows full angular resolution, i.e. differential sputtering yield measurements are measured as a function of both polar angle and azimuthal angle. Measured profiles are presented for 100, 250, 350 and 500 eV Xe+ bombardment at 0º, 15º, 30º and 45º angles of incidence. We fit the measured profiles with Modified Zhang expressions using two free parameters: the total sputter yield, Y, and characteristic energy E*. Sputtering of HBC versus HBR grades of BN is compared, as is results of sputter measurements from the weight loss versus QCM approaches. Finally, effects of sample moisture absorption are considered.

Nomenclature

A_s	=	QCM sensor area
E_b	=	Binding energy
E^*	=	characteristic energy to describe sputtering profile
J	=	ion current
R	=	easured mass accumulation rate
r_{qcm}	=	distance from the target to the QCM
y	=	differential sputter yield
Y	=	total sputter yield,
α	=	QCM sensor polar angle from target normal
β	=	ion incidence angle from target normal
ϕ	=	azimuthal angle in the target plane from the plane containing the ion beam and target normal
ρ	=	density of target material

I. Introduction

Ion sputtering is the process in which atoms (and molecules, clusters, or ions) are ejected from the surface of material due to bombarding incident ions. Our primary interest is to better understand the role of sputtering in electric propulsion (EP) thrusters used for satellite and space exploration[1-7]. In these devices, sputter erosion of grids and other components places a fundamental limitation on lifetimes. Additionally, sputtered particles from within the

* Post-Doctoral Researcher, Mechanical Engineering, brubin@engr.colostate.edu
† Graduate Student, Mechanical Engineering, jim.Topper@colostate.edu
‡ Assistant Professor, Mechanical Engineering, ayalin@engr.colostate.edu

thrusters or from external spacecraft components can redeposit and contaminate spacecraft surfaces (e.g. thermal control surfaces). From the point of view of erosion (and contamination) in Hall thrusters, boron nitride (BN) is generally the material of primary interest. More specifically, BN is widely used as an insulator material in the acceleration channel of stationary plasma thrusters (SPTs). However, despite the importance of BN erosion there is a lack of fundamental sputtering data on BN.

A partial list of measurement techniques for total and differential sputter yield includes: weight loss[8], collector plates[9-10], mass spectrometry[11], quartz crystal microbalance[2-6,12-14], Rutherford backscattering[15-16], radioactive tracers[17], and cavity ring-down spectroscopy[18]. In this contribution we present sputter measurements of BN obtained by both weight loss and the quartz crystal microbalance (QCM). The QCM is an angularly resolved measurement giving information on the differential sputter yield; however, the QCM can only measure condensable sputtering components (e.g. boron atoms, but not nitrogen atoms). By combining the weight loss and QCM measurements we obtain data on both total and differential sputter yields. The measured yields can be used as inputs (and to aid validation) for numeric codes that model sputter erosion (lifetime) and/or effects of sputter redeposition. The current measurement system builds upon our previous work using a quartz crystal microbalance (QCM) for sensitive measurements of angularly resolved differential sputter yields [4-6, 12].

Ion sputtering in EP applications is generally by low energy ions (keV and below). At these conditions, stopping is predominantly due to elastic (nuclear) collisions and the sputtering is generally in the linear cascade regime (emitted particles are secondary or higher generation recoils) or single knock-on regime (emitted particles are primary recoils)[19]. A classical theory for the linear cascade regime was originally developed by Sigmund[20]. Independent of ion incidence angle, the original theory predicts sputtering profiles that are azimuthally symmetric and approximately diffuse in shape, corresponding to cosine-like profiles of the form $y \propto \cos(\alpha)^n$ (n=1 for a diffuse profile). More recent theories, as well as experimental and numerical studies show a range of profile shapes. For normally incident ions on polycrystalline and amorphous targets, cosine-like profiles are generally observed with increasingly under-cosine shapes as ion energy is lowered and increasingly over-cosine shapes for higher ion energies[4-5,11-12,21-23]. In comparison to a diffuse profile, an under-cosine profile (n<1) has less sputtering in the surface normal direction and correspondingly more sputtering (with the maximum) at intermediate angles. Conversely, an over-cosine profile (n>1) has increased sputtering (and the maximum) in the surface normal direction. For obliquely incident ions at relatively high ion energy, observed profiles also tend to be azimuthally symmetric. However, for lower ion energies the measured profiles tend to be asymmetric with increased sputtering in the forward direction[4-5,11-12,17,21]. Similar profiles have been modeled on a theoretical basis[24-26].

In Section II of this paper we summarize experimental aspects including the samples and an overview of the weight loss system and QCM apparatus including recent improvements. We also describe the use of Modified Zhang (MZ) expressions as a means to describe the measured profiles. In Section III we present results of total sputter yield measurements for HBC and HBR grades of BN. In Section IV we present results of differential sputter yield measurements for HBC and HBR grades of BN obtained from the QCM system. Measurement conditions (for both total and differential yields) are ion energies of 100, 250, 350, and 500 eV, and incidence angles of 0, 15, 30, and 45 degrees. Section V includes discussion of moisture (absorption effects) as well as comparison of our measurements to the limited existing measurements for these materials. Where possible, total sputter yields found from integration of the differential sputter yield profiles are compared with published values as well as weight loss values obtained in our laboratory. Finally, conclusions are given in Section VI.

II. Experimental

A. Materials

Test results reported herein are for HBC and HBR grades of Boron Nitride (BN). Both materials were originally obtained from General Electric's (GE's) Advanced Ceramics and correspond to the graphite-like allotrope of BN. The HBC and HBR grades are both formed by hot-pressing. Calcium borate is used as binder in HBR, no binder used in HBC. The two grades have generally similar properties though with some differences, for example, HBR has higher thermal expansion, higher moisture absorption, and higher volume resistivity at elevated temperatures. All targets are poly-crystalline (random grain orientations) so that crystallographic orientation effects are not observed. More detail on the materials can be obtained from GE datasheets.

As will be further discussed in Section V the moisture absorption effects are particularly important. The behavior is shown in Fig. 1 (from GE Website). In a humid environment (e.g. 100% relative humidity, left of Fig. 1), both types of BN pick up approximately 1% moisture (by weight) after prolonged exposure. On the other hand there is a large difference in behavior at lower humidity (e.g. 45% relative humidity, right of Fig. 1). In this case,

after initial moisture exposure and after long measurement times, the HBC BN has very low moisture pick up (approximately zero) while the HBR BN maintains approximately 1% moisture (by weight). Generally our laboratory humidity is approximately 30%, though the moisture exposure history of the samples prior to arrival in our laboratory is unclear. Given this situation, it is reasonable to expect that the HBC BN samples will have essentially no moisture pick up, but the HBR samples may have up to 1% pickup. Our measurements of HBR show varying sputter yields depending on the amount of bake-out which we attribute to (varying) moisture absorption effects. For EP interest, particularly after long exposure, we view that measurements of "dry" samples are of primary interest, so we attempt to control our sample preparation (and bake-out) in order to achieve such conditions.

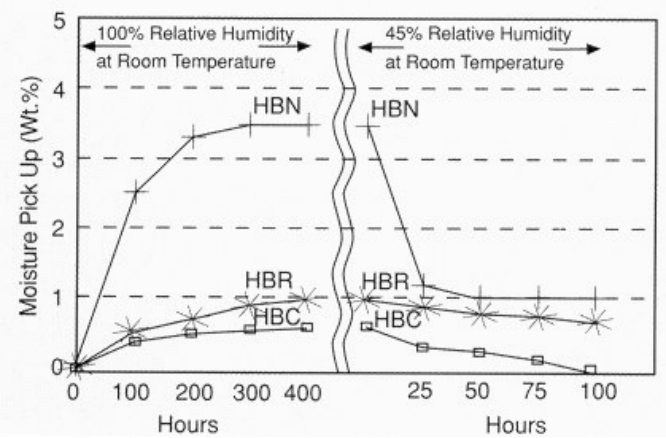

Figure 1. Moisture absorption of various grades of hot-pressed boron nitride (from GE Webpage).

B. Weight Loss Measurement System

The weight loss system has been previously described [8]. Here, we summarize the system and provide updates on system improvements. The weight loss measurements are carried out in a SPECTOR ion beam system (Ion Tech, Inc.). The 1000-liter SPECTOR chamber uses a CTI-400 cryogenic pump, and is equipped with a 16-cm diameter ion source. To ensure an accurate assessment of the sputtering behavior, a thorough characterization of the ion beam current density profile was conducted [8]. Knowledge of the incident current is needed in the sputter yield computation. The ion current density profiles were measured on several planes at four axial locations between the ion source exit plane and the plane where the samples were located. The ion current density profiles were integrated to determine the total ion current that passes each axial plane, and these values were plotted as a function of axial position to determine the effects of scattering and charge exchange. The analysis was done to allow a calculation of the total flux of fast particles (ions and neutrals) that impinge upon the samples, since both ions and fast neutral particles cause sputtering. An example of a radial distribution of total current density (i.e. ions and fast neutrals) at the target plane (z = 38 cm), as well as the measured ion current is shown in Fig. 2. In this case, at the target plane the measured (integrated) ion current was 140 mA, yielding a total fast particle current of 203 mA, the difference of

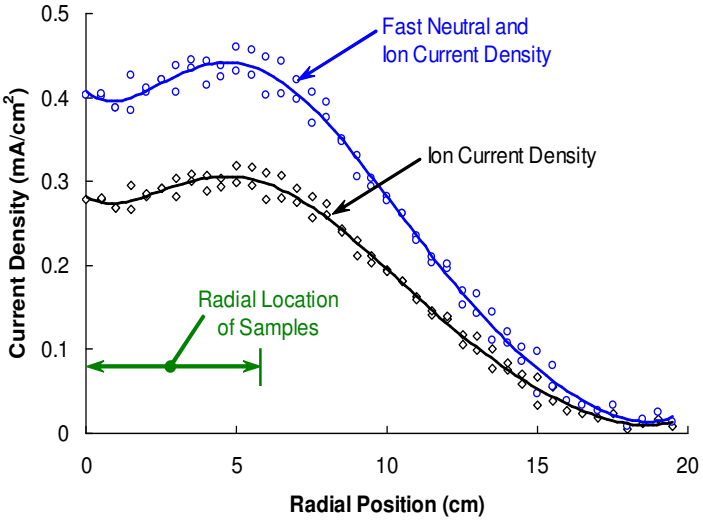

Figure 2. Total fast particle current density at the target plane. Note that the objects sputtered during these tests were placed at radial locations between 0 cm and 6 cm.

62 mA represents the fast neutral equivalent current. The equivalent current loss between source and target due to the scattering of ions and fast neutrals was estimated to be ~52 mA, i.e., 255 mA – 203 mA.

The BN samples used were typically 1-inch squares. Details of sample holders and alignment were previously reported [8]. For measurement at different incidence angles the sample holders are angled at 0˚, 30˚, 45˚, 60˚, and 75˚. Following alignment of the sample holder, the vacuum system was closed and pumped down to a pressure below $5x10^{-5}$ Torr. The quartz heaters installed within the SPECTOR vacuum facility were turned 'on' and the temperature of the sample holder was slowly raised to 150°C. The samples were baked for 10 hours. After which, they were pre-cleaned with a 350 eV, 200 mA xenon ion beam for 1.5 hours. After pre-clean, the chamber was back-filled with nitrogen, and the samples were placed into an acrylic chamber that was positively pressurized with a constant purge of nitrogen.

A microgram scale was used to weigh the samples (before and after each sputtering session). Only one sample holder was removed from the apparatus at a time, keeping unmeasured samples in the N_2 environment. Each sample was weighed 5 times (obtaining an average) and returned to the nitrogen environment. The samples were then realigned with the incident angle alignment jig and placed inside the vacuum chamber on the cooling plate, where they were again aligned with the center of the beam and the system subsequently pumped down. A 100˚C, 0.5-hour bake-out was executed, and then the system was allowed to pump down to a chamber pressure below $5x10^{-7}$ Torr. The samples were then exposed to the xenon ion beam at prescribed test conditions for periods of approximately 20 hours (depending on the expected erosion rate).

Since surface charging effects were observed for BN (see discussion in next section), plasma bridge neutralizer (PBN) was used to neutralize the surface of the samples.

C. Quartz Crystal Microbalance Measurement System

In deposition mode, the QCM allows determination of differential sputter yields through measurement of mass accumulation (of sputtered particles) on its surface. Mass changes are inferred from changes in the resonant frequency of the crystal. Knowing the change of mass, incident dose of ions, and geometry, the differential sputter yield can be simply calculated. The experimental apparatus is shown in Fig. 3. The system has been previously described[4-6,12], in this subsection we give an overview of its features and recent modifications. The ion source and QCM are housed within a 0.125 m^3 stainless steel vacuum chamber (43 cm ID x 76 cm long main section), equipped with a 1500 liter/s CTI-8 cryogenic pump. The chamber pressure was monitored using thermocouple gauge and hot cathode ionization gauge. The chamber base pressure was 5×10^{-7} Torr (after an 8-hour bake out prior to measurements) giving a working pressure of approximately 0.6 to 1×10^{-4} Torr. The ion source is based on a discharge chamber operated with xenon gas at typical flowrates of 0.3 to 0.6 sccm. A tungsten hot-filament cathode ionizes the neutral gas and a two-grid ion optic system extracts and focuses the ion beam onto the target. Neutralization of the beam and surface charging effects are addressed below. The discharge voltage (V_D) was set between 30 V and 38 V to minimize the number of multiply charged ions produced. Full-width-at-half-maximums (FWHMs) of the ion beams were in the vicinity of 3 cm (at target plane) with peak current densities of approximately 0.3 mA/cm^2 and average current densities (over the area containing 90% of the beam current) of approximately 0.1 mA/cm^2 (see Ref. 4).

A rotatable target-mount is positioned 23 cm downstream of the ion source. Compumotor motion control system is used to rotate target mount and the QCM mount. LabView program running on the PC is used to control the motion of QCM and target and to log the measurement data.

Prior to measurements, new targets were baked for 0.5 hour at 100˚ degrees and then sputter-cleaned for 3-6 hours with a 500 eV (~0.2 mA/cm^2) beam from the ion source. The same targets were often used in multiple tests; thus, we have deliberately studied pre-sputtered as opposed to new (un-sputtered) targets to better represent the conditions found in long-duration EP operating applications or in ground-based sputter coating tools. An order-of-magnitude estimate for the typical dose of incident ions (on the target prior to a given test) is approximately $10^{20\text{-}21}$ ions/cm^2 (corresponding to 10s-100s of hours and eroded thickness of approximately 10-100 microns). Target contamination effects are estimated to be negligible, since for typical conditions the flux of ions incident on the target is approximately 10 times higher than the flux of nitrogen (the major contaminant) to the target[12].

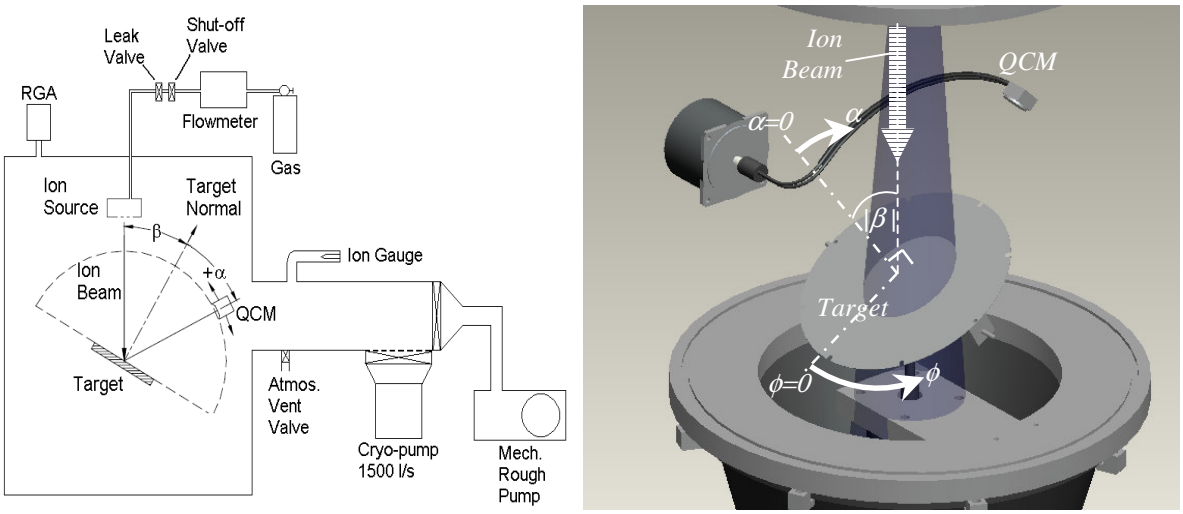

Figure 3. Schematic diagram of experimental set-up.

For improved measurement sensitivity we have obtained a Sigma Instrument SQC-339 Deposition Controller that reads the crystal frequency to 0.01 Hz. Also, for improved sensitivity and accuracy a new advanced RC-cut QCM was obtained instead of the conventional AC-cut QCM. The RC-cut QCM manufactured by Tangidyne Corporation is extremely accurate for deposition of very thin films. High sensitivity is achieved by adjusting the stress coefficients of the quartz plate using advanced fabrication methods. We have also upgraded our temperature controller to a Polyscience 9000 series digital temperature controller that allows temperature control to better than 0.01 K. Prior to use of this controller we had observed short-term rippling in the (apparent) mass deposition which was found to be correlated with slight temperature variation in the QCM cooling loop. The effect of the rippling was to degrade our ability to determine the slope, thereby degrading measurement accuracy and sensitivity. At typical conditions, the new temperature controller has improved sensitivity by a factor of approximately 3. For most materials of interest, the new upgraded QCM system enables measurement of differential sputter yield at ion energies as low as 50-100 eV.

In our measurements of insulators, e.g. boron nitride, we have observed effects of surface neutralization on the measured sputter yields[6]. Surface charging effects on BN sputtering have been previously observed by Zhang et al.[27] In order to neutralize the surface charge, a plasma beam neutralizer (PBN) was placed in the chamber close to the sample being sputtered. As an example, Fig. 4a shows the dependence of the HBC grade Boron Nitride sputter yield on the beam current at fixed beam voltage (prior to PBN installation). The reduction in sputter yield with increasing beam current was attributed to surface charging of the BN surface. At higher beam current more positive charge is accumulated on the sample surface and the charge repels beam ions thus reducing the measured sputter yield. These measurements were performed for 500 eV xenon ions at normal incidence with the QCM polar angle at 40 degrees from the surface normal. Measurements of the sputter yield versus beam current with PBN operating are shown on Fig. 4b. The dependence of the sputter yield on the beam current is significantly reduced. Similar PBN neutralization is employed in both the QCM and Weight Loss systems. The operating conditions of PBN used in QCM system are: emission current = 10-20 mA, Xe mass flow rate = 0.5 sccm. The PBN was biased negatively relative to ground potential and was set equal to the ion source neutralizer potential (typically -24 V).

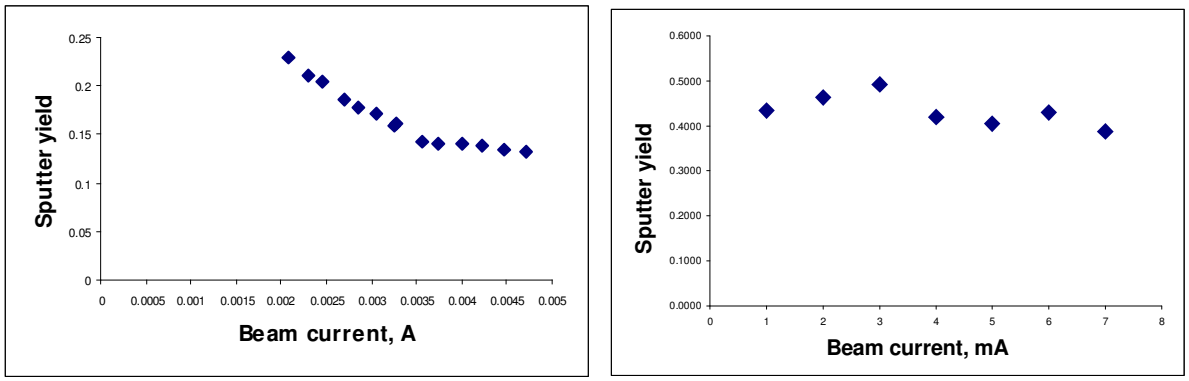

a **b**

Figure 4: Sputter yield versus beam current before (a) and after (b) PBN installation

The angles used to describe the direction of ion incidence and the ejections angles of sputtered particles are shown in Fig. 3. We define as follows: β is the incidence angle of bombarding ions measured relative to the surface normal (β=0 for normal incidence), α is the ejection polar angle of sputtered atoms measured relative to the surface normal, and ϕ is the ejection azimuthal angle of the sputtered atoms measured in the plane of the target surface (defined so that ϕ=0 is in the forward sputter direction i.e. in the direction of the plane containing the surface normal and the incident ion directions). For a given incidence angle (obtained by tilting the target), the differential sputtering profile is obtained by measuring the sputter yield at a series of angles above the target: ~X polar angle positions over Y azimuthal slices.

At a given measurement point, the volumetric differential sputter yield, $y(\alpha,\phi)$, is determined using Eq. (1), in which $R(\alpha,\phi)$ is the measured mass accumulation rate (found from a deposition monitor device), ρ is the density of target material, $J_{B,avg}$ (C/s) is the ion current incident on the target (measured every 0.5 s and averaged), r_{qcm} the distance from the target center to the QCM (17.4 cm), and A_s is the QCM sensor area (0.535 cm^2). The quantity A_s/r_{qcm}^2 corresponds to the solid angle that the QCM sensor subtends while $R(\alpha,\phi)/\rho J_{B,avg}$ corresponds to the volume of sputtered material per bombarding charge. The resulting $y(\alpha,\phi)$ is in units of volume/charge/steradian (e.g. mm^3/C/sr):

$$y(\alpha,\phi) = \left[R(\alpha,\phi) r_{qcm}^{\,2} \right] \Big/ \left[\rho J_{B,avg} A_s \right] \tag{1}$$

As a means to describe the measured differential (angular) sputter yield profiles we adopt the use of Modified Zhang (MZ) expressions [6,12]. The availability of such expressions is limited; however Zhang[26] have published expressions for differential sputter yield profiles. Zhang's expressions are improvements of earlier expressions from Yamamura [24-25]:

$$y_{MZ} = \frac{Y}{1-\sqrt{\frac{E^*}{E}}\cos(\beta)} \cdot \frac{\cos(\alpha)}{\pi} \left[1 - \frac{1}{4}\sqrt{\frac{E^*}{E}} \left(\cos(\beta)\gamma(\alpha) + \frac{3}{2}\pi \sin(\beta)\sin(\alpha)\cos(\phi) \right) \right] \tag{2a}$$

$$\gamma(\alpha) = \frac{3\sin(\alpha)^2 - 1}{\sin(\alpha)^2} + \frac{\cos(\alpha)^2 \left(3\sin(\alpha)^2 + 1\right)}{2\sin(\alpha)^3} \ln\left(\frac{1+\sin(\alpha)}{1-\sin(\alpha)} \right) \tag{2b}$$

where y_{MZ} is the differential sputter yield, Y is the total sputter yield, E is the ion energy, E^* is a characteristic energy describing the profile shape, and the angles are as define above. The approach decouples the amplitude of the angular profiles from their shape, through the use of Y and respectively. More recent work by Zhang et al[28] also discusses the use of a varying energy parameter, but in the context of expressions for energy distributions and total

sputter yields. In general, rather than using the MZ expressions for *a priori* calculation, we treat Y and E^* as free fit-parameters which we determine from (least-squares fitting) experimental data. As shown below, the best-fit values of characteristic energy E^* vary with ion energy and incidence angle and generally do not equal the threshold energy for sputtering. Note that for high ion energy (limit $E>>E^*$) the MZ expression reduces to the diffuse yield ($y=Y\cos(\alpha)/\pi$).

III. Results & Discussion

A. A. Total Sputter Yields (Weight Loss)

Validation measurements of our weight loss system were reported in past publications [6,12]. Most such measurements were for xenon ions on molybdenum for which the total sputter yields were very comparable with published measurements from other groups. In this section the total sputter yield measurements of HBC and HBR grades of BN are presented. Further discussion is in Section IV.

Figures 5 and 6 show the measured total sputter yields for HBC and HBR grades of BN. The plots are versus ion incidence angle and are for measurement conditions of ion energy of 100, 250, 350, and 500 eV, and incidence angles of 0˚, 30˚, 45˚, 60˚, and 75˚.

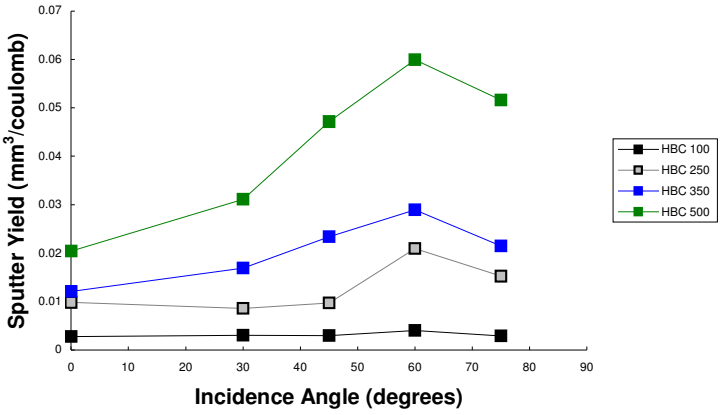

Figure 5. Total sputter yield versus incidence angle for HBC BN.

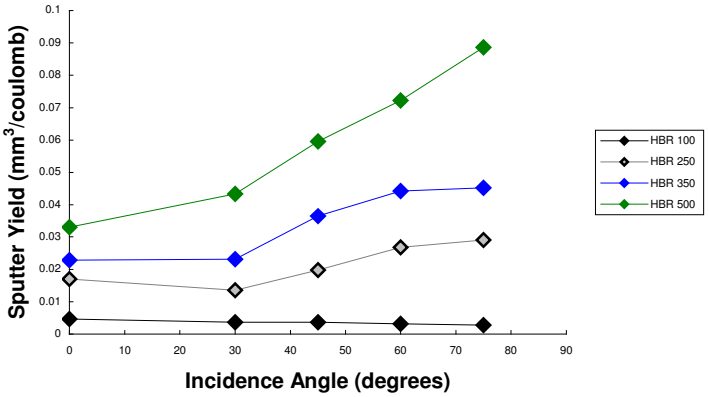

Figure 6. Total sputter yield versus incidence angle for HBR BN.

Where possible, we compare the measured yields with those from the limited published measurements. Figure 7a shows our HBC and HBR 350 eV measurements along with weight loss measurements by a Garnier et al[29] and a profilometry measurement by Britton et al[30] at similar energy. Neither author specifies the grade of BN used. We

view the agreement with other data as reasonable especially given possible material variation, surface effects etc. Figure 7b shows comparison with measurements by Garnier[29] at 500 eV and also shows reasonable agreement. Note that the lowest sputtering energies reported in these comparison studies were 300 eV by Britton[30] and 350 eV by the Garnier[29], and apart from our own work we are not aware of other measurements below 300 eV. It is interesting to note that sputter yield of HBR is about 1.5-2 times higher than HBC yield.

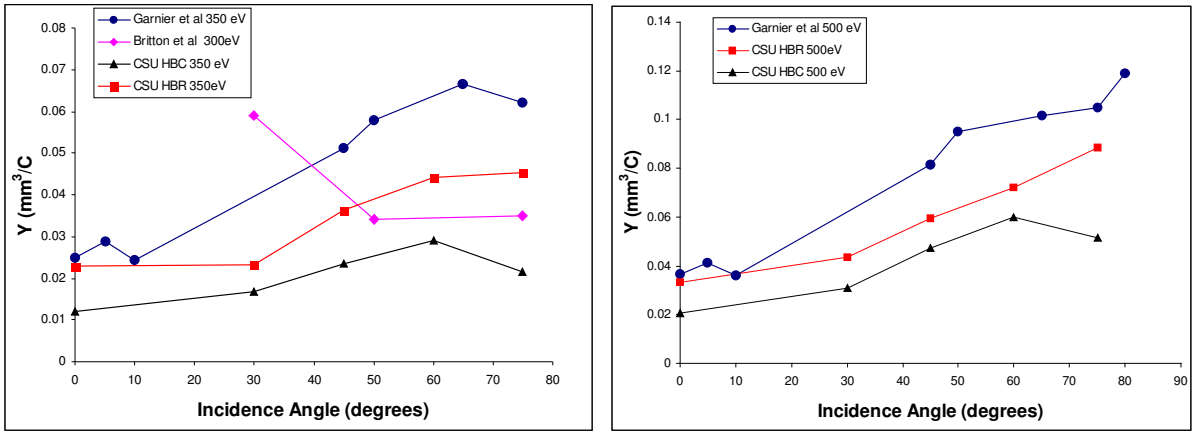

a **b**

Figure 7. Total BN sputter yields as compared with published values

B. Differential Sputter Yields (Quartz Crystal Microbalance)

Table 1 provides results of the differential sputter yield measurements for HBC and HBR grades of BN. The measured profiles are for 100, 250, 350 and 500 eV Xe^+ bombardment at 0º, 15º, 30º and 45º angles of incidence. The measured profiles are analyzed in terms of their shapes which are described with the measured (best-fit) values of characteristic energy E^* (as discussed above). Additionally, to characterize the agreement between the fitted MZ profiles and the measured data, we also provide an error column, which we compute as the average (absolute) difference between the measured points and corresponding fitted points, normalized by the maximum measured yield.

Table 1. Characteristic Energies (E^*) and Total Sputter Yields (Y) of HBC and HBR BN

Ion Energy (eV)	Incidence Angle (Deg)	HBC: E^* (eV)	*HBC:* Error	HBR: E^* (eV)	*HBR:* Error
100	0	19	0.22	1	0.135
100	15	18	0.10	2	0.251
100	30	18	0.10	7	0.105
100	45	14	0.14	6	0.164
250	0	42	0.27	37	0.136
250	15	65	0.13	58	0.133
250	30	96	0.12	69	0.087
250	45	86	0.12	97	0.143
350	0	88	0.11	130	0.240
350	15	97	0.15	130	0.127
350	30	150	0.12	140	0.124
350	45	160	0.12	180	0.134
500	0	120	0.10	190	0.163
500	15	150	0.13	210	0.132
500	30	210	0.11	250	0.134

Examples of comparison between measured (raw) QCM data and fitted MZ profiles are given in Fig. 8 (in arbitrary units). Both plots are for xenon ion energies of 250 eV on HBR BN, with the left plot being at normal incidence and the right plot being at 30 degrees incidence. The plots include: QCM measured points, best-fit MZ profiles, and (for comparison) diffuse profiles with the same total yield. One can see relatively good agreement between the measured profiles and MZ profiles (see also numerical error values in Table 2). The normally incident profile is azimuthally symmetric. The profile for 30 degrees incidence is measured in the forward/backward plane (ϕ=0,180 degrees) and shows a forward sputter lobe (negative alpha) and reduced sputtering in the backward direction (positive alpha). We find that the MZ expressions provide a reasonable description of the measured profiles, but tend to predict a slightly broader and lower amplitude forward-sputter lobe. Qualitatively, the results for HBC BN, and for other angles and energies for HBR BN are similar.

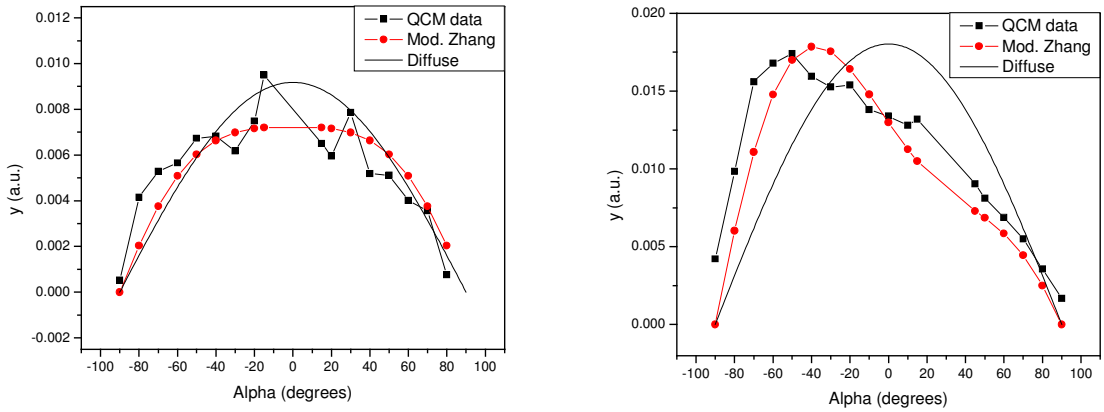

Figure 8. Example of QCM data with best-fit MZ profiles for 250 eV ions on HBR BN. Left: Normal incidence. Right: 30 degrees incidence.

In Fig. 9-10 we plot (using colored hemispheres) the best-fit Zhang differential sputter yields for each of the measured cases. Colors (indicated in legend) correspond to the yield in the given direction. Here we focus on the shape (not magnitude) of the profiles; therefore, we normalize the differential sputter yields by the total sputter yields (or equivalently assume total sputter yields of unity). Comparison of Fig. 9 and 10 shows that the shapes of the differential sputter yield profiles for HBC and HBR grades of BN are qualitatively similar. A similar conclusion can be reached by noting that the E* values for HBR and HBC are relatively similar (generally within ~10-30%) of one another for the two materials.

The QCM measurement approach also provides total sputter yields (through fit parameter Y). For HBC BN the values are reliable but tend to be higher than the corresponding values from weight loss. Given that the QCM measures only condensable components, one would expect if anything for the QCM to have lower values. The reasons for this discrepancy are under investigation. It should be noted that in other sputter yield studies with QCM similar effect – systematically high absolute sputer yields calculated from QCM data – was observed [31]. In our past measurements of molybdenum sputtering Mo we find good agreement between weight loss and QCM results. Interestingly, other researchers have seen similar discrepancy in the case of BN (REF). For HBR BN, the total sputter yield measurements (overall signal amplitudes) are less reliable owing to limitations of the QCM bake-out system (and associated moisture effects). We have, however, verified that for different bake-outs the shapes of the profiles remain consistent so that the values of E* should not be affected. Effects of moisture on HBR sputter yields are discussed in the following section.

C. Moisture Effects

During the course of our measurements we have observed variations in HBR sputter yields owing to what we attribute to effects of moisture absorption. As discussed in Section IIA, HBR BN can maintain appreciable amounts of moisture even after storage in a dry environment. Figure 11 shows QCM measurements of HBR BN at normal incidence and fixed ion energy of 500 eV. The lowest (blue) curve corresponds to measurements without prior bake-out; the medium (purple) curve corresponds to 0.5 hour long bake-out at 100 C, the highest (yellow) curve corresponds to 2-hour bake-out at 100 ˚C with following 2-hour bake-out at 150 ˚C. Note that in each case we pre-

sputter the targets with 500 eV ion beam for at least 1 hour, yet the sputtering is observed to be insufficient to restore the surfaces to their original conditions. We do not observe any analogous variation in sputter yield for HBC BN.

Based on these observations we conclude that the moisture pickup is affecting the sputter yields of HBR BN. The exact mechanism is unclear but it is postulated that the surface undergoes chemical or compositional changes causing a change in sputter yields. For EP interest, particularly after long exposure, we view that measurements of "dry" samples are of primary interest, so in the work reported here we have attempted to control our sample preparation (and bake-out) in order to achieve such conditions. As is apparent from Fig. 11, increased bake-out leads to increased yields.

During the weight loss measurements, mass variation of HBR sample caused by absorption was observed. Weight of HBR samples was increasing during approximately one hour each time the samples were exposed to atmosphere after. The weight measurements were taken after the weight of the samples reached steady-state (it was checked that the weight increase is approximately the same for different samples). Similar effect was reported by Garnier[29].

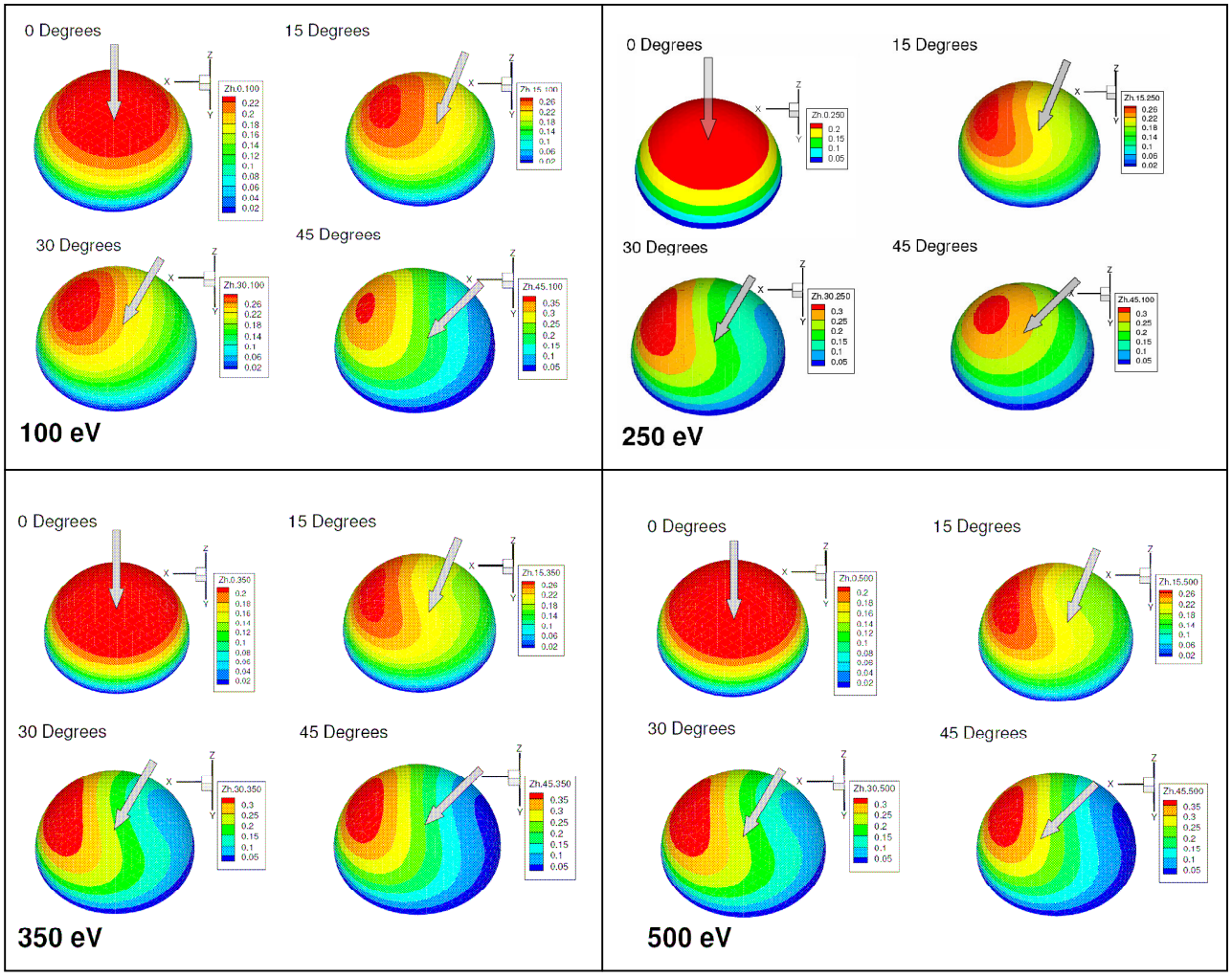

Figure 9. Normalized differential sputter yield profiles for xenon ions on HBC BN.

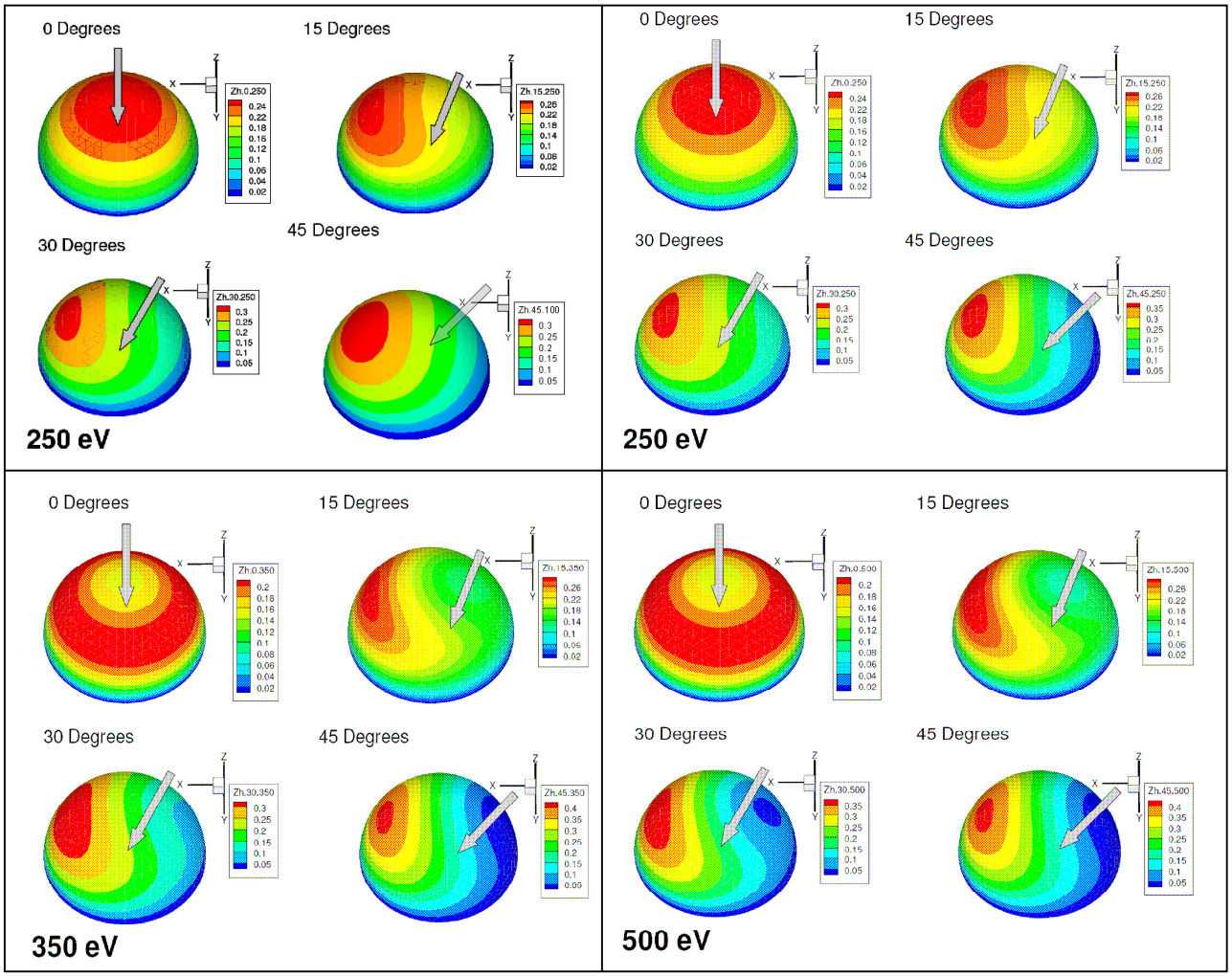

Figure 10. Normalized differential sputter yield profiles for xenon ions on HBR BN.

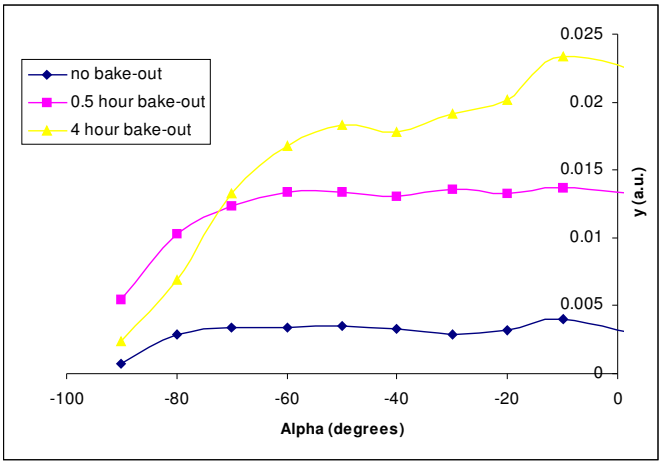

Figure 11. Measured sputter yield profiles of HBR BN for different bake-out sample preparation conditions.

IV. Conclusions

We have reported total and differential sputter yield measurements for HBC BN using our weight loss and QCM measurement systems respectively. Total sputter yields show reasonable agreement with those in the literature, though published values are unavailable below 300 eV and our measurements at these lower energies are the first. In terms of comparison of HBC and HBR total yields, we find that the total yields for HBR BN are approximately 1.5-2 times higher. Angular dependence is similar expect for the most oblique angle studied .

With the exception of our recently reported HBC BN differential sputter yields[6], the measurements reported here are the first differential sputter yields of BN. The MZ profiles provide a reasonable description of the measured profiles. In summary, the shapes (E* values) for HBC BN and HBR BN are relatively similar showing azimuthally symmetric behavior at normal incidence and forward/backward sputtering features at oblique incidence.

Future measurement needs for BN include:

- Studies of dependence of sputter yields on target temperature (possible with QCM modification)
- Studies of the moisture effect on HBR BN sputter yield
- Studies at lower ion energies (possible with specialized grid-sets using QCM and CRDS detection)
- Studies of other grades of BN (HBR BN in progress, others possible)
- Further validation studies and investigation of condensable fraction by comparison of QCM with weight loss (ongoing and future work).

Acknowledgments

The research was funded by Air Force Research Laboratory, Edwards Air Force Base.

References

[1] Tartz M., Neumann H., Fritsche B., Leiter H., and Esch J., "Investigation of Sputter Behavior of Ion Thruster Grid Materials", *40th Joint Propulsion Conference,* AIAA Paper 2004-4114.

[2] Kolasinski, R. D., "Oblique Angle Sputtering Yield Measurements for Ion Thruster Grid Materials", *41st Joint Propulsion Conference,* AIAA paper 2005-3526.

[3] Kolasinksi, R. D., Polk, J. E., Goebel, D. and Johnson, L. J., "Carbon sputtering yield measurements at grazing incidence", *42nd AIAA/ASME/SAE/ASEE Joint Propulsion Conference*, AIAA paper 2006-4337.

[4] Zoerb, K. A., Williams, J. D., Williams, D. D., and Yalin, A. P., "Differential sputtering yields of refractory metals by xenon, krypton, and argon ion bombardment at normal and oblique incidences", *29th International Electric Propulsion Conference,* IEPC paper 2005-293.

[5] Yalin, A. P., Williams, J. D., Surla, V., Wolf, J., and Zoerb, K. A., "Azimuthal differential sputter yields of molybdenum by low energy Xe^+ bombardment", *42nd AIAA/ASME/SAE/ASEE Joint Propulsion Conference,* AIAA paper 2006-4336.

[6] Yalin, A.P., Rubin, B., Domingue, S.R., Glueckert, Z., and Williams, J.D., "Differential Sputter Yields of Boron Nitride, Quartz, and Kapton Due to Low Energy Xe^+ Bombardment", *43rd AIAA/ASME/SAE/ASEE Joint Propulsion Conference,* AIAA paper 2007-5314.

[7] Surla, V.K., Tao, L., Yalin, A.P., "Species-Specific Measurements with Cavity Ring-Down Spectroscopy", *43rd AIAA/ASME/SAE/ASEE Joint Propulsion Conference,* AIAA paper 2007-5315.

[8] Yalin, A.P., Surla, V., Farnell, C., Butweiller, M., and Williams, J.D., "Sputtering Studies of Multi-Component Materials by Weight Loss and Cavity Ring-Down Spectroscopy", *42nd AIAA/ASME/SAE/ASEE Joint Propulsion Conference,* AIAA paper 2006-4338.

[9] Chiplonkar, V. T., and Rane, S. R, "Dependence of Angular Distribution of Sputtering by Positive Ions from Metal Targets on the Impact Angle", *Indian Journal of Pure and Applied Physics*, Vol. 3, 1965, p. 161.

[10] Tsuge, H. and Esho, S., "Angular Distribution of Sputtered Atoms from Polycrystalline Metal Targets", *Journal of Applied Physics*, Vol., 52, No.7, 1981, pp 4391-4395.

[11] Wucher, A., and Reuter, W., "Angular Distribution of Sputtered Particles from Metals and Alloys", *Journal of Vacuum Science and Technology A,* Vol. 6, No. 4, 1988, pp. 2316-2318.

[12] Yalin, A.P., Williams, J.D., Surla, V., and Zoerb, K. A., "Differential Sputter Yield Profiles of Molybdenum due to Bombardment by Low Energy Xenon Ions at Normal and Oblique Incidence", accepted to *Journal of Physics D – Applied Physics (2007)*.

[13] Mannami, M., Kimura, K., and Kyoshima, A. "Angular Distribution Measurements of Sputtered Au Atoms with Quartz Oscillator Microbalances", *Nuclear Instruments and Methods,* Vol. 185, 1981, pp. 533-537.

[14] Wickersham, C. E., and Zhang, Z., "Measurement of Angular Emission Trajectories for Magetron-sputtered Tantalum", *Journal of Electronic Materials*, Vol. 34, No.12, 2005.

[15] Shutthanandan, V., Ray, P., Shivaparan, N., Smith, R., Thevuthasan, T. and Mantenieks, M. "On the Measurement of Low-energy Sputtering Yield Using Rutherford Backscattering Spectrometry", *25th International Electric Propulsion Conference* , IEPC paper 97-069.

[16] Mantenieks, M., Foster, J., Ray, P., Shutthanandan, S., and Thevuthasan, T., "Low Energy Xenon Ion Sputtering Yield Measurements", 27th International Electric Propulsion Conference, IEPC paper 01-309.

[17] Kundu, S., Ghose, D., Basu, D., Karmohapatro, S. B., "The Angular Distribution of Sputtered Silver Atoms", *Nuclear Instruments and Methods in Physics Research B,* Vol. 12, No.3, 1986 pp. 352-355.

[18] Yalin, A.P., Surla, V., Butweiller, M., Williams, J.D., "Detection of Sputtered Metals using Cavity Ring-Down Spectroscopy", *Applied Optics*, Vol. 44, No. 30, 2005, pp. 6496-6505.

[19] Betz, G., and Wien, K., "Energy and angular distributions of sputtered particles", *International Journal of Mass Spectrometry and Ion Processes,* Vol. 140, No.1, 1994 pp. 1-110.

[20] Sigmund, P., "Theory of Sputtering I: Sputtering Yield of Amorphous and Polycrystalline Targets", *Physical Review* Vol. 184, No.2, 1969 pp. 383-416 .

[21] Wehner, G. K., and Rosenberg, D., "Angular Distribution of Sputtered Material", *Journal of Appied Physics*, Vol. 31, 1960, pp. 177-179.

[22] Chini, T. K., Tanemura., M., and Okuyama., F. "Angular Distribution of Sputtered Ge Atoms by Low keV Ar+ and Ne+ Ion Bombardment", *Nuclear Instruments and Methods in Physics Research B,* Vol. 119, 1996, pp. 387-391.

[23] Yamamura, Y., and Muraoka, K., "Over-cosine Angular Distributions of Sputtered Atoms at Normal Incidence", *Nuclear Instruments and Methods in Physics Research B,* Vol. 42 1989, pp. 175-81.

[24] Yamamura, Y., "Contribution of Anisotropic Velocity Distribution of Recoil Atoms to Sputtering Yields and Angular Distributions of Sputtered Atoms", *Radiation Effects and Defects in Solids,* Vol. 55, No.1, 1981 pp. 49–55.

[25] Yamamura, Y., "Theory of Sputtering and Comparison to Experimental Data", *Nuclear Instruments and Methods,* Vol., 194, 1982, pp. 515–522.

[26] Zhang, Z. L., and Zhang. L, "Anisotropic Angular Distributions of Sputtered Atoms", *Radiation Effects and Defects in Solids*, Vol. 159, No. 5, 2004, pp. 301-307.

[27] Zhang, J., Bhattacharjee, S., Shutthanandan, V., and Ray, P. K., "Sputtering Investigation of Boron Nitride with Secondary Ion and Secondary Neutral Mass Spectrometry", *Journal of Vacuum Science and Technology A,* Vol. 15, No. 2, 1997, pp. 243-247.

[28] Zhang, L., and Zhang, L., Z., 2005 "Anisotropic Energy Eistribution of Sputtered Atoms Induced by Low Energy Heavy Ion Distribution", *Radiation Effects and Defects in Solids*, Vol. 160, pp. 337-347.

[29] Garnier, Y., Viel, V., Roussel, J.-F., and Bernard, J., "Low-energy Xenon Ion Sputtering of Ceramics Investigated for Stationary Plasma Thrusters", *Journal of Vacuum Science and Technology A,* Vol.17, No. 6., 1999, pp. 3246-3254.

[30] Britton, M. Waters, D., Messer, R., Sechkar, E., and Banks, B., "Sputtering Erosion Measurements on Boron Nitride as a Hall Thruster Material", NASA/TM 2002-211837, 2002.

[31] Behrisch, R. (ed.), *Sputtering by Particle Bombardment I*, Springer-Verlag, Berlin,1981, p.153.